nature immunology

SUPPLEMENTARY INFORMATION

https://doi.org/10.1038/s41590-018-0132-0

In the format provided by the authors and unedited.

Blockade of the checkpoint receptor TIGIT prevents NK cell exhaustion and elicits potent anti-tumor immunity

Qing Zhang[1,2], Jiacheng Bi[2,3], Xiaodong Zheng[2], Yongyan Chen[2], Hua Wang[4], Wenyong Wu[4], Zhengguang Wang[4], Qiang Wu[4], Hui Peng[2], Haiming Wei[1,2], Rui Sun[1,2]* and Zhigang Tian[1,2]*

[1]Hefei National Laboratory for Physical Sciences at Microscale, University of Science and Technology of China, Hefei, Anhui, China. [2]Institute of Immunology and The CAS Key Laboratory of Innate Immunity and Chronic Disease, School of Life Sciences and Medical Center, University of Science and Technology of China, Hefei, Anhui, China. [3]Shenzhen Laboratory of Fully Humanized Antibody Engineering, Institute of Biomedicine and Biotechnology, Shenzhen Institutes of Advanced Technology, Chinese Academy of Sciences, Shenzhen, China. [4]the First Affiliated Hospital of Anhui Medical University, Hefei, Anhui, China. *e-mail: sunr@ustc.edu.cn; tzg@ustc.edu.cn

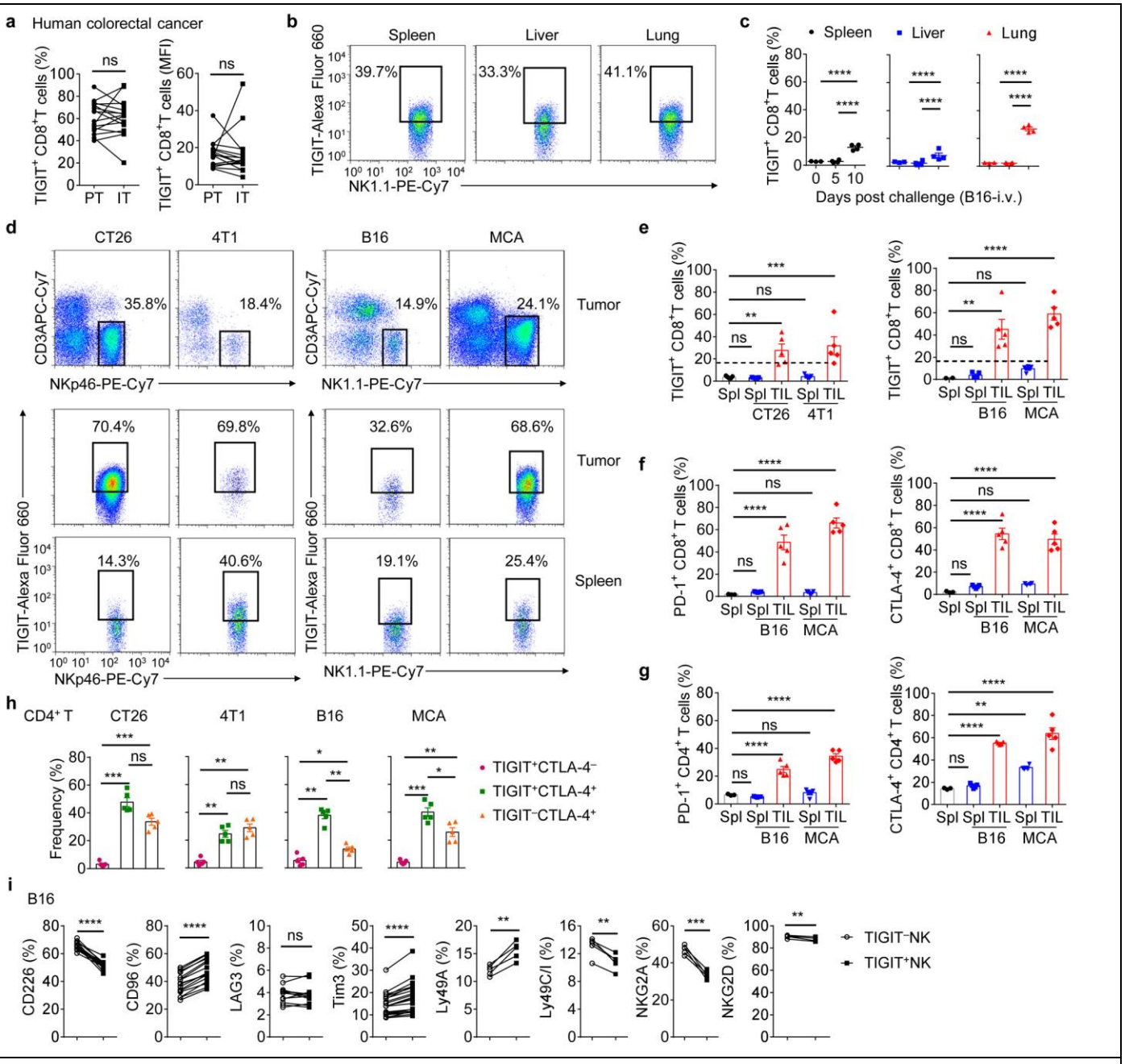

Supplementary Figure 1

Phenotypes of tumor-infiltrating lymphocytes.

Supplementary Figure 1. Phenotypes of tumor-infiltrating lymphocytes. (**a**) Frequency and MFI of TIGIT$^+$ cells in CD8$^+$ T cells (CD45$^+$CD3$^+$CD56$^-$) from peritumoral regions (PT) and intratumoral regions (IT) in patients with CRC (n=16). (**b**) Representative flow cytometry plot of TIGIT expression in NK cells from the spleen, liver and lung as described in Figure 1b. (**c**) Frequencies of TIGIT$^+$ in CD8$^+$ T cells in B16-pulmonary metastasis model (n=4 mice per group). (**d**) Representative flow cytometry plots of tumor-infiltrating NK cells and TIGIT expression on NK cells in four subcutaneous tumor models. (**e**) Frequencies of TIGIT$^+$ cells in CD8$^+$ T cells as described in Figure 1c (n=5 mice per group). (**f, g**) Frequencies of PD-1$^+$, or CTLA-4$^+$ cells in CD8$^+$ or CD4$^+$ T cells as described in Figure 1d (n=5 mice per group). (**h**) Frequencies of TIGIT$^+$CTLA-4$^-$, TIGIT$^+$CTLA-4$^+$, and TIGIT$^-$CTLA-4$^+$ cells in tumor-infiltrating CD4$^+$ T cells (n=5 mice per group). (**i**) Frequencies of CD226, CD96, LAG3, TIM3, Ly49A, Ly49C/I, NKG2A and NKG2D (n=16, 16, 15, 23, 5, 5, 5, 5 mice) in TIGIT$^-$ and TIGIT$^+$ tumor-infiltrating NK cells in B16-pulmonary metastasis model. (**b-i**) Data are representative of at least three independent experiments. ns, not significant ($P > 0.05$), *$P < 0.05$, **$P < 0.01$, ***$P < 0.001$, ****$P < 0.0001$; Error bars are

mean ± s. e. m. (**c, e, f, g**); paired two-tailed *t*-test (**a, i**); one-way ANOVA followed by Tukey's (**c, h**) or Dunnett's (**e, f, g**) multiple comparisons test.

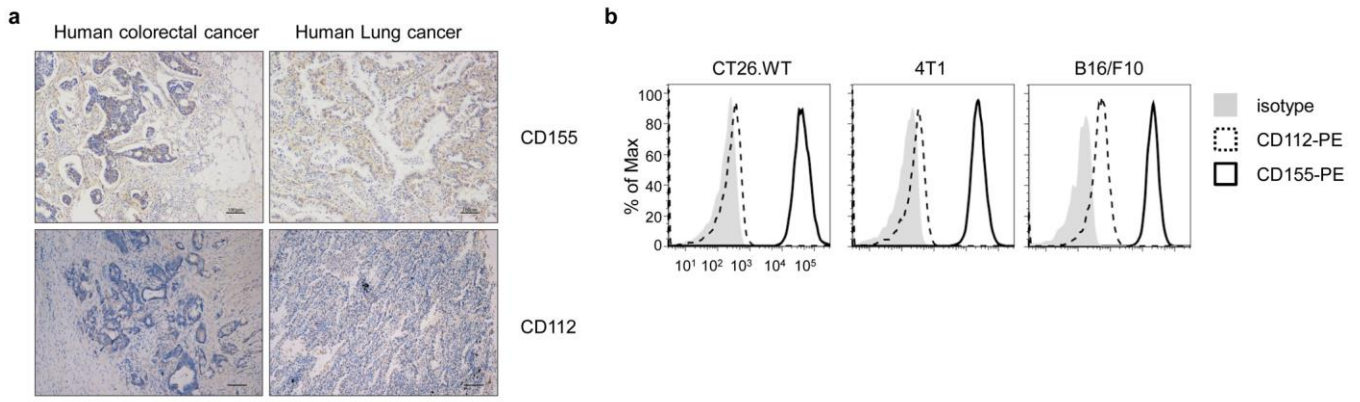

Supplementary Figure 2

The TIGIT ligand CD155 is abundant in human and murine tumors.

(**a**) Representative images of immunolabeling for CD155 and CD112 in human tumor tissues (paraffin sections from 20 tumor patients with colorectal cancer or lung cancer). Scale bars are 100 μm. (**b**) The expression of CD155 and CD112 on tumor cells we used in the murine tumor models. (**a, b**) The experiment was repeated independently for four times with similar results.

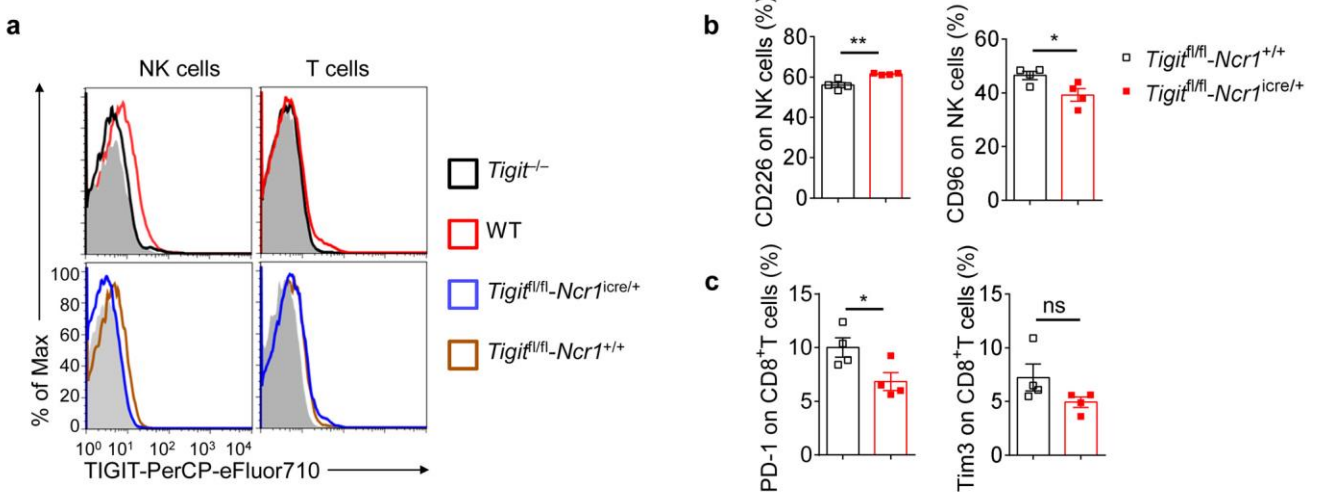

Supplementary Figure 3

Conditional knockout of TIGIT on NK cells prevents the exhaustion of TILs.

(**a**) Representative histograms of TIGIT expression on NK and T cells from *Tigit*$^{fl/fl}$- *Ncr1*$^{iCre/+}$, *Tigit*$^{fl/fl}$- *Ncr1*$^{+/+}$, *Tigit*$^{-/-}$ and WT mice. Grey shadow represent isotype staining. The experiment was repeated independently for three times with similar results. (**b, c**) *Tigit*$^{fl/fl}$-*Ncr1*$^{iCre/+}$ and *Tigit*$^{fl/fl}$- *Ncr1*$^{+/+}$ mice were intravenously injected with 1.5×10^5 B16/F10 cells (n=4). TILs were analyzed 15-d post challenge. (**b**) Expression of CD226 and CD96 in tumor-infiltrating NK cells. (**c**) Expression of PD-1 and Tim3 in tumor-infiltrating CD8$^+$ T cells. (**b-c**) Data are representative of three independent experiments. ns, not significant ($P > 0.05$), *$P < 0.05$, **$P < 0.01$; Error bars are mean ± s. e. m. (**b, c**); unpaired two-tailed *t*-test (**b, c**).

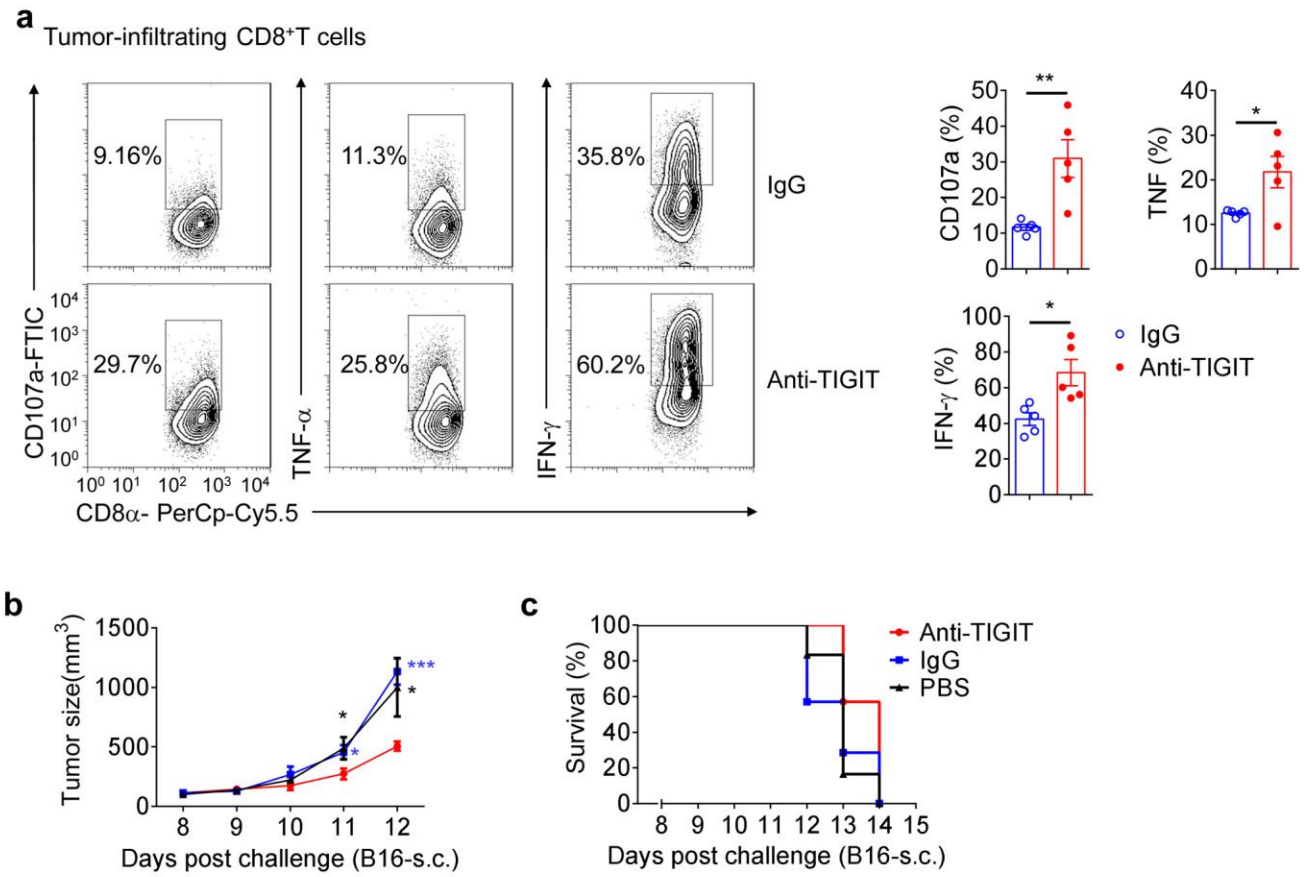

Supplementary Figure 4

TIGIT blockade alone inhibits tumor growth and reverses the exhaustion of tumor-infiltrating $CD8^+$ T cells.

(**a**) Expression of CD107a, TNF, and IFN-γ in tumor-infiltrating $CD8^+$ T cells in CT26-tumor bearing mice (n=5 mice per group). (**b, c**) B16 melanoma model. Mice were subcutaneously injected with 5×10^4 B16/F10 cells, and treated with anti-TIGIT mAb and control IgG for 3 times (once every 3 d). (**b**) Tumor size over time (anti-TIGIT, IgG, PBS, n=6, 5, 4 mice). (**c**) Survival of mice (anti-TIGIT, IgG, PBS, n=7, 7, 6 mice). Data are representative of three (**a**) or two (**b, c**) independent experiments. $^*P < 0.05$, $^{**}P < 0.01$, $^{***}P < 0.001$; Error bars are mean ± s. e. m. (**a, b**); unpaired two-tailed *t*-test (**a**); multiple *t* tests (**b**); Mantel-Cox test (**c**).

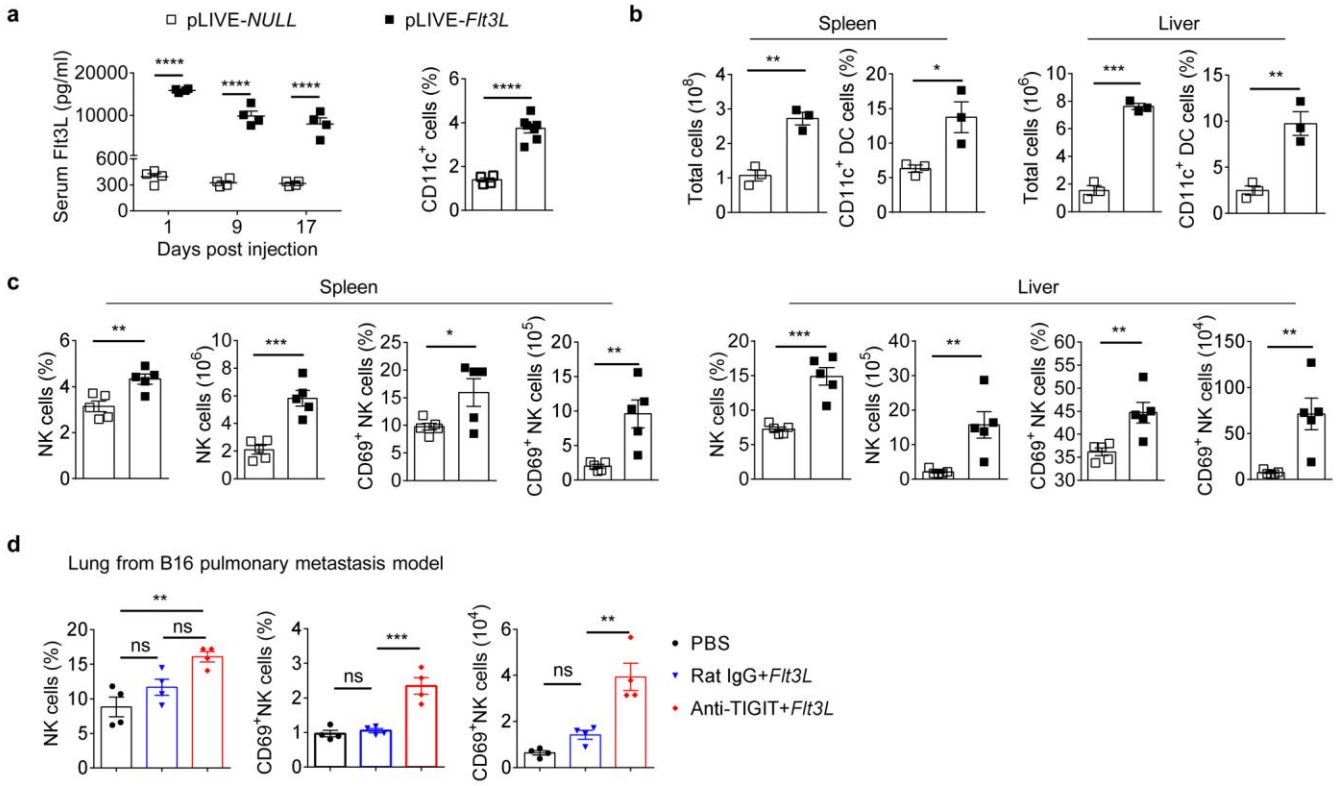

Supplementary Figure 5

pLIVE-*mFlt3L* injection accumulates DCs and NK cells, and promotes the activation of NK cells.

(**a-c**), Mice were hydro-dynamically injected with 10 μg pLIVE-*mFlt3L* or pLIVE-*NULL*. Serum was collected at indicated time post injection. The peripheral blood was collected from the tail vein 2 weeks after the injection. Splenic and Hepatic cells were isolated 4 weeks after the injection. (**a**) Soluble Flt3L level in serum (n=4 mice per group) and the frequency of DCs in PBMC (pLIVE-*NULL*, pLIVE-*Flt3L*, n=4, 7 mice). (**b**) The frequency and absolute numbers of DCs cells in spleen and liver (n=3 mice per group). (**c**) The frequency and absolute numbers of NK cells and $CD69^+$ NK cells in spleen and liver (n=5 mice per group). (**d**) The frequency of NK cells, $CD69^+$ NK cells and absolute number of $CD69^+$ NK cells in lung from B16 pulmonary metastasis model. Mice were treated as described in Figure.3n (n=4 mice per group). (**a-d**) Data are representative of three independent experiments. ns, not significant ($P > 0.05$), *$P < 0.05$, **$P < 0.01$, ***$P < 0.001$, ****$P < 0.0001$; Error bars are mean ± s. e. m. (**a-d**); Two-way ANOVA followed by Sidak's multiple comparisons test (**a** left); unpaired two-tailed *t*-test (**a** right, **b, c**); one-way ANOVA followed by Tukey's multiple comparisons test (**d**).

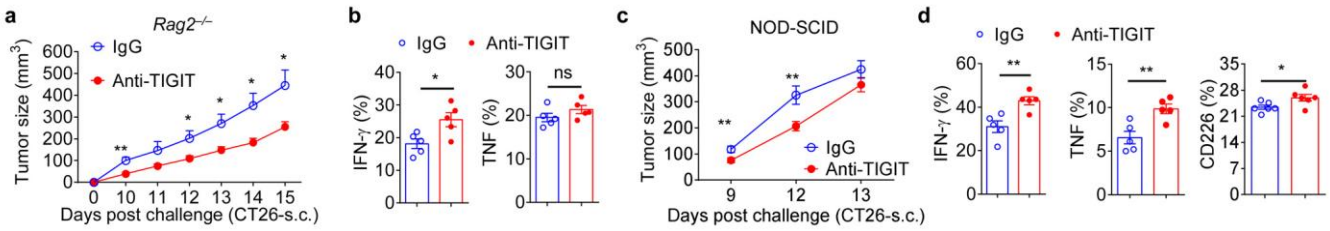

Supplementary Figure 6

TIGIT blockade inhibits tumor growth in *Rag2*$^{-/-}$and NOD-SCID mice.

(**a, c**) Tumor size over time (*Rag2*$^{-/-}$, IgG, anti-TIGIT, n=6, 6; NOD-SCID, IgG, anti-TIGIT, n=16, 18). (**b, d**) Expression of IFN-γ (n=5 mice per group), TNF (n=5 mice per group) and CD226 (n=6 mice per group) in tumor-infiltrating NK cells. (**a-d**) Data are representative of two independent experiments. ns, not significant ($P > 0.05$), *$P < 0.05$, **$P < 0.01$; Error bars are mean ± s. e. m. (**a-d**); multiple *t* tests (**a, c**); unpaired two-tailed *t*-test (**b, d**).

Supplementary Table 1
Details of patients with colorectal cancer (CRC).

Case ID	Sample	Age at Diagnosis	Gender	Stage at first diagnosis	Site of primary tumor	Prior treatment
CRC1	Primary tumor	38	F	II	Colon	Untreated
CRC2	Primary tumor	74	M	IV	Colon	Untreated
CRC3	Primary tumor	78	M	I	Colon	Untreated
CRC4	Primary tumor	51	M	III	Rectum	Untreated
CRC5	Primary tumor	64	F	III	Rectum	Untreated
CRC6	Primary tumor	63	M	II	Colon	Untreated
CRC7	Primary tumor	48	F	III	Colon	Untreated
CRC8	Primary tumor	68	M	I	Rectum	Untreated
CRC9	Primary tumor	72	F	II	Colon	Untreated
CRC10	Primary tumor	53	F	III	Colon	Untreated
CRC11	Primary tumor	37	F	II	Colon	Untreated
CRC12	Primary tumor	64	F	III	Colon	Untreated
CRC13	Primary tumor	44	F	III	Rectum	Untreated
CRC14	Primary tumor	42	F	III	Colon	Untreated
CRC15	Primary tumor	80	M	II	Rectum	Untreated
CRC16	Primary tumor	67	M	I	Rectum	Untreated
CRC17	Primary tumor	62	F	IV	Colon	Untreated
CRC18	Primary tumor	44	M	III	Rectum	Untreated
CRC19	Primary tumor	64	M	IV	Colon	Untreated